Hydrodynamic cavitation in minifluidic Venturi nozzle

Radek Zeman[1*] and *Pavel* Rudolf[1]

[1]Victor Kaplan Dept. of Fluid Engineering, Faculty of Mechanical Engineering, Brno University of Technology, Technická 2896/2, 616 69 Brno, Czech Republic

Abstract. This article describes the design of a small Venturi nozzle for hydrodynamic cavitation wastewater treatment research. A water circuit powered by compressed air was set up for the experiment. The nozzle design allowed visualization of the cavitating flow directly in the nozzle using a high-speed camera. Experiments were carried out with the nozzle to obtain a visualization of the flow and the dependence of the loss coefficient on the cavitation number. Furthermore, computational modeling of the flow was performed based on the results obtained in the experiment. Cavitation could play an important role in removing pollutants from water that cannot be removed by conventional methods in water treatment plants. The ability to process large quantities of water is one of the great advantages of hydrodynamic cavitation, however, when testing the influence of cavitation on pollutants contained in water, the need for large quantities of tested water appears unnecessary, impractical, and expensive. Research is still needed to better understand the effects of cavitation on water purification, and small-scale experiments may be more suitable for this kind of task.

1 Introduction

Cavitation is known primarily for its negative effects on pump and turbine impellers, causing cavitation erosion, vibration, and noise. However, new fields of application are emerging for cavitation, where it is no longer seen as a negative and unwanted phenomenon. One of the investigated applications of cavitation is water purification [1,2]. Viruses, bacteria, pharmaceuticals, various organic substances, and other pollutants are of interest [3]. For the needs of hydrodynamic cavitation research, cavitation reactors are used, most often in the form of a Venturi nozzle [4,5]. Efforts are being made to determine the effect of cavitation on these impurities in water and whether cavitation can effectively neutralize them or at least reduce their content. Kosel et al. [6] investigated the effect of cavitation on the deactivation of the MS-2 virus contained in water. Due to the problematic multiplication of the virus and its limited occurrence in the environment, a small cavitation reactor working with only 3 ml of water was built for the experiment. To check the validity of the cavitation experiment on such a small scale, a larger cavitation reactor working with 1 liter of water was used. Virus inactivation was observed in both cavitation reactors, making the smaller reactor more suitable for analysis with smaller sample volumes. The use of small hydrodynamic cavitation reactors in the form of a nozzle or orifice has already been used in several studies [7,8,9]. The nozzle design within this paper was inspired by the work of Pobevšek et al. [10] and the paper itself is based on a master's thesis of Zeman [11].

2 Experiment

2.1 Nozzle fabrication

The nozzle was part of an assembly consisting of a 0.5 mm thick stainless steel plate, two acrylic glass plates, and a paper gasket. The shape of the nozzle was machined by electrical discharge machining (EDM) into sheet metal. The sheet metal was then sandwiched between sheets of acrylic glass. To ensure tightness, two 0.05 mm thin paper gaskets were used, into which the shape of the nozzle was also cut. The gaskets were placed between the sheet metal plate and the plexiglass plates. The whole assembly was fitted with holes along the edge, into which a screw connection was then placed, thus the whole assembly was firmly joined together. The dimensions of the sheet metal are shown in Figure 1.

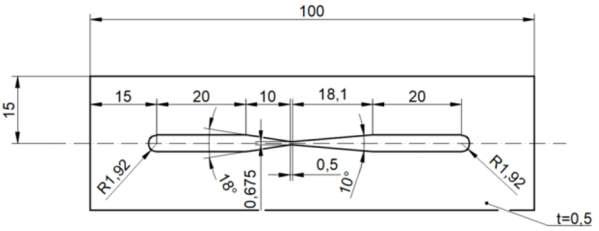

Fig. 1. Dimensions of the sheet metal**.**

The nozzle had a rectangular cross-section with a constant depth of 0.6 mm, the depth was formed by the thickness of the sheet and two paper gaskets. The nozzle neck was 0.5 mm long and 0.675 mm wide. The

* Corresponding author: 192038@vutbr.cz

converging and diverging angles of the nozzle were 18° and 10° respectively. Upstream and downstream of the nozzle were 20 mm straight sections with a constant width of 3.84 mm. Holes were drilled at the ends of the channel to insert ports for tubing connection. The complete assembly is shown in Figure 2.

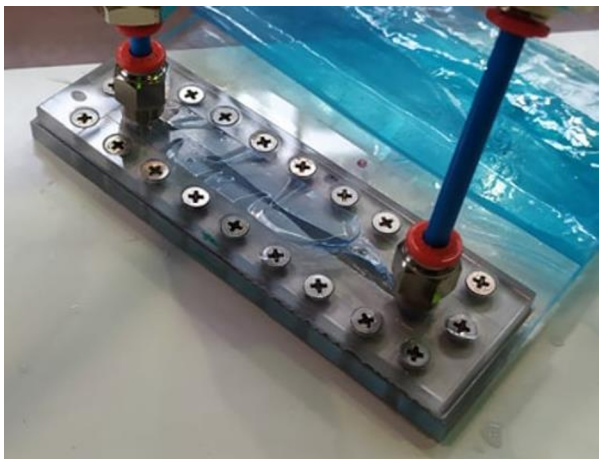

Fig. 2. Nozzle assembly.

2.2 Experimental circuit

A water circuit was built for the experiments, consisting of a pressure vessel, tubing, valves, fittings, and pressure gauges. The pressure vessel with a maximum capacity of 4 liters could be filled with tap water or pressurized with compressed air via valves. After passing the nozzle, the water was discharged through a hose with a second pressure gauge into the atmosphere. Pressure gauges were placed 30 mm upstream and downstream of the nozzle assembly. The flow behind the nozzle throat could be monitored by a high-speed camera. The circuit scheme is shown in Figure 3.

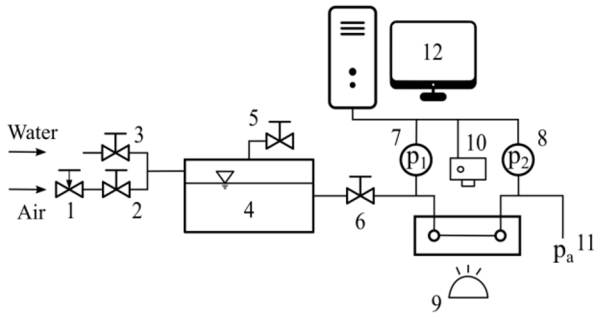

Fig. 3. Circuit scheme, (1) control valve, (2,3,5,6) valves, (4) pressure vessel, (7,8) pressure gauges, (9) light source, (10) high-speed camera, (11) discharge to atmosphere, (12) data acquisition.

Before each measurement, the pressure vessel had to be vented and refilled with water. Then compressed air could be released into the vessel while the pressure value was adjusted by the control valve. The water was pushed by compressed air into the nozzle through a shut-off valve and a pressure gauge. The flow rate through the circuit had to be measured as the mass of fluid that flowed through the circuit over the measured period.

2.3 Experimental results

A total of 14 points were measured from which a nozzle characterization was made. The experiments were performed with tap water at flow rates ranging from 5 to 15 ml/s. Cavitation number σ was defined by the relation:

$$\sigma = \frac{p_2 - p_V}{\rho \cdot \frac{v^2}{2}} \; [1] \qquad (1)$$

Where p_2 is the pressure downstream of the nozzle, p_V is the saturation vapor pressure of water for a given temperature, ρ is the density of the water, and v is the mean flow velocity in the nozzle throat.

The loss coefficient was defined by the relation:

$$\xi = \frac{p_1 - p_2}{\rho \cdot \frac{v^2}{2}} \; [1] \qquad (2)$$

where p_2 is the pressure upstream of the nozzle.

The characteristics of the nozzle are shown in Figure 4.

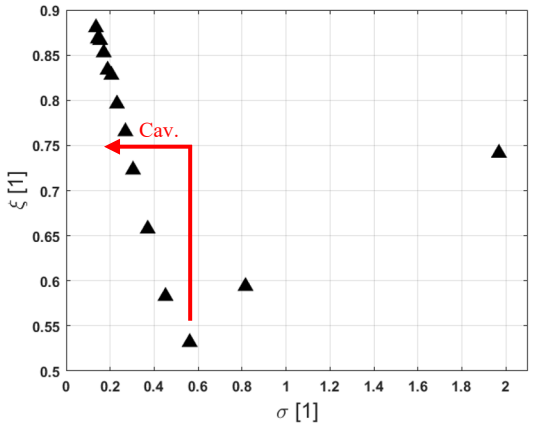

Fig. 4. Nozzle characteristics.

The graph shows a decrease in the loss coefficient with decreasing cavitation number. This decrease was probably due to flow at low values of the Reynolds number through hydraulically smooth internal surfaces. The onset of cavitation was determined at the point where the value of the loss coefficient begins to rise sharply with decreasing cavitation number. The loss coefficient was increasing until it was no longer possible to increase the pressure in the pressure vessel because the maximum permissible pressure (7 bar absolute pressure) had been reached.

A visualization for each measured point is shown in Figure 5.

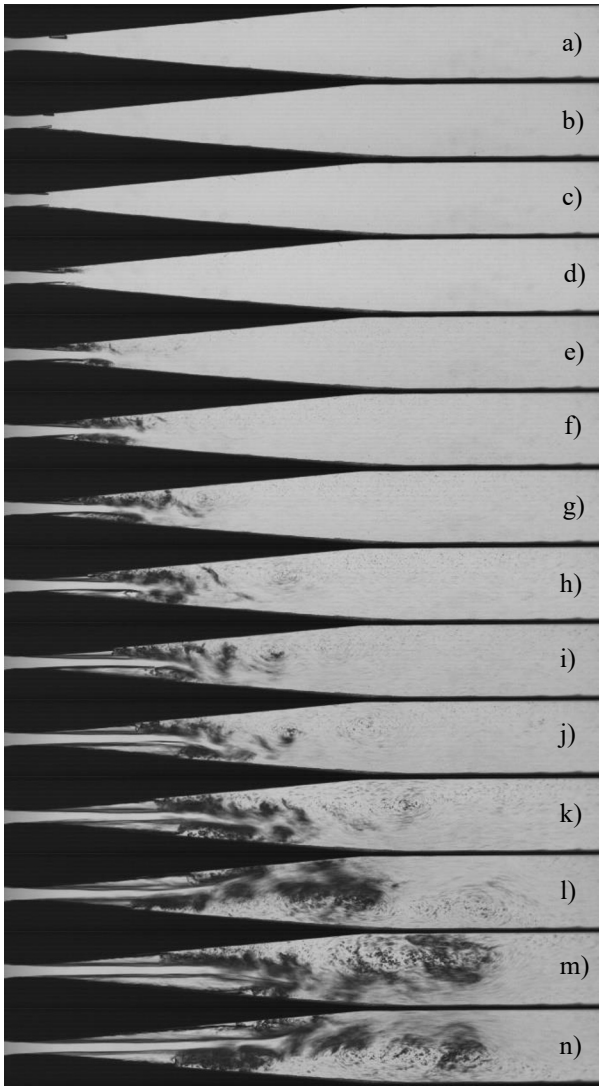

Fig. 5. Visualization, a) σ=1,969, b) σ=0,816, c) σ=0,562, d) σ=0,452, e) σ=0,371, f) σ=0,304, g) σ=0,269, h) σ=0,231, i) σ=0,206, j) σ=0,188, k) σ=0,171, l) σ=0,155, m) σ=0,144, n) σ=0,135.

The visualization showed the presence of cavities already at the highest measured cavitation numbers, however, these bubbles in the nozzle throat were probably caused by the expulsion of gases dissolved in water during the pressure drop, therefore this regime was not considered cavitation. The onset of cavitation occurred between cavitation numbers (c) and (d) when small bubbles of saturated water vapor could already be observed to break off from the two cavities present in the nozzle throat. With decreasing cavitation number, cavities grew in length and larger cavitation structures disintegrated, forming a vortex containing bubbles of saturated water vapor. The flow was very dynamic, unstable, and asymmetrical. Detachment of the end of the cavity caused shrinkage of the cavity and subsequent regrowth, these phenomena were periodically repeated. The cavitation in the nozzle was accompanied by acoustic effects in the form of noise increasing with increasing cavitation intensity.

The asymmetry in the cavitating flow is probably caused by the presence of the Kelvin-Helmholtz instability, previously observed and described by Podbevšek et al. [10]. The presence of shear flow at the boundary between the cavities and the fluid flow causes vorticity at the end of the cavities and their subsequent detachment as vortices. Kelvin-Helmholtz instability was probably also the reason for the highly asymmetric flow in the nozzle, which is visible in all images of the cavitating flow. This type of asymmetric flow is typical for diffusers with large divergence angles [12].

3 Numerical simulation

3.1 Geometry and mesh

The numerical simulation was performed in Ansys Fluent. 2D geometry and subsequently a 2D hexahedral structured mesh with 78 240 elements were created for the calculation. The geometry contained only the internal chip assembly, short sections of tubing leading to the pressure gauges were neglected here, as well as local loss due to the bending of the flow.

3.2 Simulation settings

The boundary conditions for the calculation were the flow velocity at the inlet to the fluid domain, which was calculated from the experimental measurement results. Atmospheric pressure was set as the pressure boundary condition at the fluid domain outlet. A transient multiphase calculation with a homogeneous mixture of water and saturated vapor with the Schnerr-Sauer cavitation model was used. The SIMPLE algorithm was used for pressure-velocity coupling. For spatial domain discretization, second-order upwind was used for all variables except the phase fraction, where the QUICK scheme was used. A time step of 1.10^{-5} s with 15 iterations per time step was chosen for the calculation. SST-k-ω was used as the turbulence model, with the turbulent viscosity adjusted using a user-defined function, which reduces the turbulent viscosity value in areas where cavitation occurs. Turbulent viscosity was adjusted according to the relation:

$$f(\rho) = \rho_V + \alpha^n(\rho_L - \rho_V)\ [kg.m^{-3}] \quad (3)$$

$$\mu_T = \frac{f(\rho)k}{\omega}\frac{1}{max\left(\frac{1}{a^*}, \frac{SF_2}{a_1\omega}\right)}\ [Pa.s] \quad (4)$$

where ρ_V is water vapor density ρ_L is water density, α is the volume fraction of the liquid in the mixture and n is the exponent of 10, k is turbulence kinetic energy, ω is specific dissipation rate, a^* is coefficient damping the turbulent viscosity, S is strain rate magnitude, F_2 is blending function, a_1 is coefficient 0,31. This turbulent viscosity adjustment was first used by Delgosha et al. [13]

3.3 CFD results

The variables monitored during the calculation were averaged and used to calculate the cavitation number and loss coefficient according to the same relationships used in the experiment. The final characteristic of the nozzle determined by CFD can be seen in figure 6.

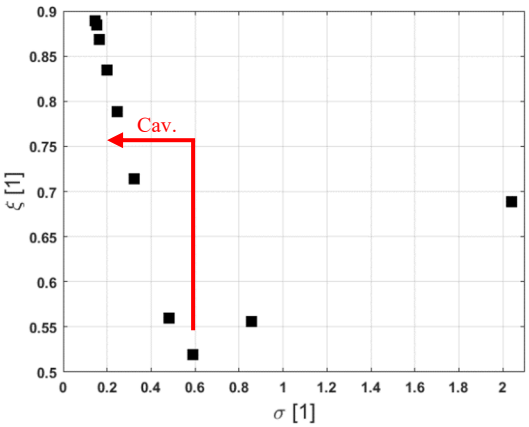

Fig. 6. Nozzle characteristics CFD

For the three points with the largest cavitation numbers, the numerical calculation was set as a single-phase because the multi-phase calculation tended to predict cavitation even at these points, while it was clear from the experimental results that cavitation should not occur.

The user-defined function for turbulent viscosity reduction resulted in cavity breakup and better mimicking of the unsteady nature of cavitation while having no significant effect on the resulting values of cavitation number and loss coefficient. The contour images of the phase fraction show that the simulation predicted a higher vapor phase content in the region downstream of the nozzle throat. The effect of UDF on the flow field can be seen in figure 7.

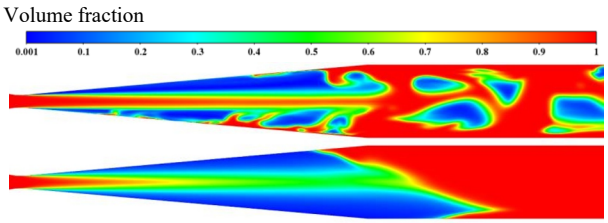

Fig. 7. Volume fraction contour with UDF (upper image) and without UDF, σ = 0,152.

4 Comparison

CFD and experimental results showed good agreement, especially in the part of the graph where cavitation occurs.

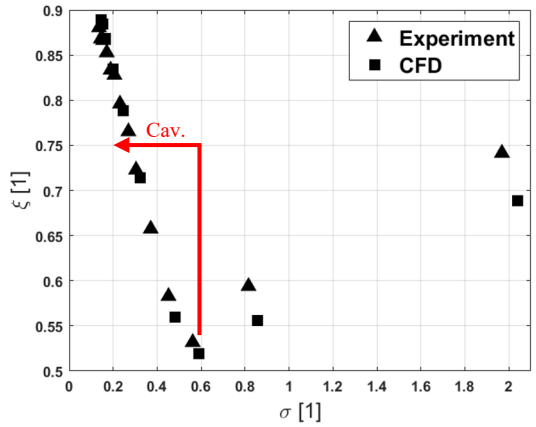

Fig. 8. Nozzle characteristics comparison.

Differences could be seen in the flow field when comparing images from the flow visualization and contours from the CFD. The use of UDF helped to simulate the unsteady nature of the cavitation, however, some phenomena were observed that were not present in the experiment:

- the simulation predicted a higher proportion of the vapor phase extending to much higher distances from the nozzle throat than the experimental visualization shows
- during the simulation, whole cavities were detached from the nozzle neck accompanied by a pressure pulse, whereas complete detachment never occurred during the experiment
- presence of cavitation in the simulation even at the highest cavitation numbers

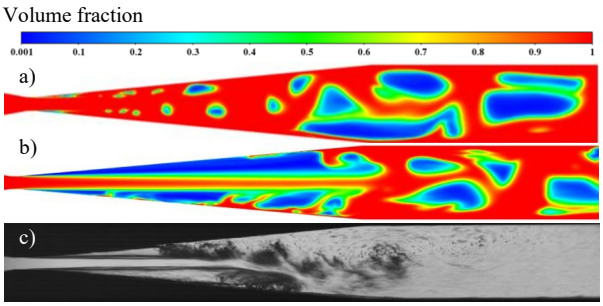

Fig. 9. Comparison of the flow field from CFD and experiment, σ=0,152, a) detachment of the cavity (UDF), b) overproduction of the vapor phase (UDF), c) visualization image.

5 Conclusion

This paper describes the design of a device containing a small Venturi nozzle. Experiments were performed and compared with CFD simulations. Good agreement was found for loss coefficient prediction in the cavitation regime. The transparent design of the device allowed visualization of the cavitating flow, which could be compared with the flow fields obtained from multiphase CFD. Application of UDF suppressing overproduction of turbulent viscosity in vapor regions significantly enhanced simulated flow dynamics. However, not all of the phenomena observed in the experiment were captured correctly in simulation, e.g., complete

detachment of cavities, pressure pulses, overproduction of the vapor phase, etc.

The experiment undoubtedly confirmed the functionality of the nozzle and the occurrence of cavitation at very low flow rates of up to 15 ml/s. Working with low flow rates may be advantageous in the future for small scale cavitation experiments and monitoring the effect of impurities in the form of particles and gas nuclei in the water on the cavitation onset and development, or monitoring the products formed during cavitation treatment.

Research was supported by Czech Science Foundation under project 22-11456S „*Exploring fundamental interactions of hydrodynamic cavitation and low-temperature plasma to enhance the disinfection effects*“ and specific research project FSI FSI-S-20-6235.

6 References

1. M. Dular, T. Griessler-Bulc, I. Gutierrez-Aguirre, E. Heath, T. Kosjek, A. K. Klemenčič, M. Oder, M. Petkovšek, N. Rački, M. Ravnikar, A. Šarc, B. Širok, M. Zupanc, M. Žitnik, B. Kompare, Ultrason. Sonochem. **29**, 577-588 (2016)
2. B. Wang, H. Su, B. Zhang, Chem. Eng. J. **412**, 128685 (2021)
3. D. Jančula, P. Mikula, B. Maršálek, P. Rudolf, F. Pochylý, Aquac. Int. **22**, 509-521 (2014)
4. J. Kozák, P. Rudolf, M. Hudec, D. Štefan, M. Forman, J. Fluids Eng. Trans. ASME **141(4)**, 1-11 (2019)
5. P. Rudolf, M. Hudec, M. Gríger, D. Štefan, EPJ Web of Conferences **67**, 02101 (2014)
6. J. Kosel, I. Gutiérrez-Aguirre, N. Rački, T. Dreo, M. Ravnikar, M. Dular, Water Res. **124**, 465-471 (2017)
7. J. Rooze, M. André, G. J. S. van der Gulik, D. Fernández-Rivas, J. G. E. Gardeniers, E. V. Rebrov, J. C. Schouten, J. T. F. Keurentjes, Microfluid. Nanofluidics **12**, 499–508 (2012)
8. M. Deggelmann, J. A. Nöpel, F. Rüdiger, D. Paustian, P. Braeutigam, Ultrason. Sonochem. **83**, 105950 (2022)
9. M. V. Bagal, P. R. Gogate, Ultrason. Sonochem. **21**, 1035-1043 (2014)
10. D. Podbevšek, M. Petkovšek, C. D. Ohl, M. Dular, Int. J. Multiph. Flow **142**, 103700 (2021)
11. R. Zeman, *Hydrodynamic cavitation in minifluidic Venturi nozzle*, Master’s thesis, VUT Brno (2022)
12. W. Albring, *Angewandte Strömungslehre* **2**, 380 (1962)
13. O. Coutier-Delgosha, R. F. Patella, J. L. Reboud, J. Fluids Eng. **125**, 38-45 (2003)